

## RESEARCH ARTICLE

10.1002/2013JD021063

## Key Points:

- Climate engineering via cirrus cloud thinning is simulated in a GCM
- Cooling can be achieved but not without climatic side effects
- Risk of remote climate changes

## Correspondence to:

H. Muri,  
helene.muri@geo.uio.no

## Citation:

Muri, H., J. E. Kristjánsson, T. Storelvmo, and M. A. Pfeffer (2014), The climatic effects of modifying cirrus clouds in a climate engineering framework, *J. Geophys. Res. Atmos.*, 119, doi:10.1002/2013JD021063.

Received 22 OCT 2013

Accepted 17 MAR 2014

Accepted article online 20 MAR 2014

## The climatic effects of modifying cirrus clouds in a climate engineering framework

H. Muri<sup>1</sup>, J. E. Kristjánsson<sup>1</sup>, T. Storelvmo<sup>2</sup>, and M. A. Pfeffer<sup>3</sup>

<sup>1</sup>Department of Geosciences, University of Oslo, Oslo, Norway, <sup>2</sup>Department of Geology and Geophysics, Yale University, New Haven, Connecticut, USA, <sup>3</sup>Icelandic Meteorological Office, Reykjavik, Iceland

**Abstract** The climatic effects of climate engineering—or geoengineering—via cirrus cloud thinning are examined. Thinner cirrus clouds can allow more outgoing longwave radiation to escape to space, potentially cooling the climate. The cloud properties and climatic effects due to perturbing the ice crystal fall speed are investigated in a set of hemispheric scale sensitivity experiments with the Community Earth System Model. It is found that increasing the ice crystal fall speed, as an analog to cirrus cloud seeding, depletes high-level clouds and reduces the longwave cloud forcing. Deliberate depletion of cirrus clouds increases outgoing longwave radiation, reduces the upper tropospheric water vapor, and cools the climate. Global cirrus cloud thinning gave a net cloud forcing change of  $-1.55 \text{ W m}^{-2}$  and a global annual mean temperature change of  $-0.94 \text{ K}$ . Though there is negligible change in the global annual mean precipitation ( $-0.001 \text{ mm/d}$ ), the spatially nonhomogeneous forcing induces circulation changes and hence remote climate changes. Climate engineering the Southern Hemisphere only results in a northward shift of the Intertropical Convergence Zone and possible Sahelian drought alleviation, while targeting the Northern Hemisphere alone causes a greater cooling. It was found that targeting cirrus clouds everywhere outside of the tropics results in changes to the circulation and precipitation even in the nonclimate engineered regions, underscoring the risks of remote side effects and indeed the complexity of the climate system.

### 1. Introduction

Climate engineering has been suggested as a tool to alleviate anthropogenic climate warming. The term climate engineering, or geoengineering, can be defined as intentionally modifying the climate in order to temporarily offset or reduce increasing surface temperatures by global warming. The idea of climate engineering has been revived due to concerns over the slow progress of climate mitigation. A number of climate engineering methods have been proposed within the main categories of radiation management and carbon dioxide removal and storage. Radiation management is introduced here as a new term and includes solar radiation management (SRM), which targets shortwave radiation and also cirrus cloud thinning, which modifies longwave radiation. Most of the radiation management techniques proposed are within the solar radiation management category, including, e.g., spaceborne solar radiation reflectors [cf. Govindasamy and Caldeira, 2000; Govindasamy et al., 2002], stratospheric sulfur injections [e.g., Crutzen, 2006; Wigley, 2006], and brightening of low-level marine clouds [e.g., Latham, 1990; Bower et al., 2006]. These methods aim to reduce the amount of solar radiation reaching the ground.

The climate engineering method addressed in this work involves the thinning of cirrus clouds and can be categorized as a form of thermal radiation management. The idea is to deplete the high and cold cirrus clouds to enable more thermal radiation to escape the Earth's atmosphere. Cirrus clouds reflect some incoming solar radiation, but this albedo cooling is smaller than the cirrus' greenhouse effect. Cirrus cloud thinning could be done by seeding cirrus-forming regions with highly effective ice nuclei to initiate heterogeneous freezing [Mitchell and Finnegan, 2009]. It is thought that cirrus clouds are mainly formed by homogeneous freezing [Kärcher and Lohmann, 2003], though recently it has been found by aircraft measurements over North America that heterogeneous freezing could be playing an important role in cirrus cloud formation [Cziczo et al., 2013]. By introducing efficient ice nuclei, one can alter the competition between homogeneous and heterogeneous freezing. Seeding the clouds facilitates the formation of larger ice crystals with higher terminal velocities, eventually falling out of the cloud, thereby depleting it. At temperatures colder than  $-40^\circ\text{C}$ , homogeneous freezing takes place at supersaturations higher than 50% with respect to ice. Heterogeneous freezing, on the other hand, requires a lower supersaturation and will therefore be favored

if sufficient ice nuclei concentrations are present. Heterogeneous freezing can hence deplete the upper tropospheric water vapor before homogeneous freezing can take place.

Water vapor has been found to be an important climate sensitivity moderator [Sanderson *et al.*, 2008]. The GCMs (general circulation models) with the most water vapor in the upper troposphere have the highest climate sensitivity. Schmidt *et al.* [2010] found that water vapor is responsible for over half of today's greenhouse effect in the atmosphere. By removing some of the water vapor, one could reduce the warming potential of the atmosphere to counteract global warming through this method.

Bismuth triiodide,  $\text{BiI}_3$ , has been suggested as possible seeding material [Mitchell and Finnegan, 2009]. It is relatively cheap (compared to, e.g., silver iodide) and nontoxic, with efficient ice nucleating properties at temperatures colder than  $-20^\circ\text{C}$  [Mitchell and Finnegan, 2009]. Bismuth is currently used in pharmaceuticals (including Pepto-Bismol), cosmetics, and metal alloys [Ojebuoboh, 1992]. It has been estimated that some 140 t of Bismuth triiodide would be needed as seeding material per year at an annual cost of \$19 million [Marshall, 2013]. Recent research has suggested that also sea salt could be a candidate for seeding of cold cirrus clouds [Wise *et al.*, 2012]. As pointed out in Mitchell and Finnegan [2009], the seeding material would have to be inefficient at warmer temperatures to avoid interference with rain-producing clouds. The method would be the most effective at nighttime, when the clouds' cooling albedo effect is nonexistent.

The method was first outlined by Mitchell and Finnegan [2009] and tested in an atmospheric general circulation model by Storelvmo *et al.* [2013]. It was found that cirrus cloud thinning could have a radiative cooling effect of  $2.5 \text{ W m}^{-2}$ . The cooling effect could be reversed, however, if the aerosol seeding concentrations are too high. Too many ice nuclei could result in more and smaller crystals than in the unseeded atmosphere and hence an increased cirrus cloud warming effect [Storelvmo *et al.*, 2013].

Cloud tuning in order to avoid climate drifts, including tuning of cirrus parameters, has often been done in GCMs. Perturbing the cirrus cloud parameters to investigate the effects on the climate has been done in a number of studies and some examples follow. Lohmann and Roeckner [1995] found from a sensitivity modeling experiment that removing the infrared effects of cirrus clouds cooled the troposphere by several degrees, and the atmospheric circulation showed a sensitivity to the changes. Perturbing the cirrus emissivity also affected the climate sensitivity of the model, showing that cirrus clouds contribute toward higher climate sensitivity. The ice crystal fall speed parameter has been investigated in both the Quantifying Uncertainties in Model Predictions and climateprediction.net perturbed physics experiments [Murphy *et al.*, 2004; Stainforth *et al.*, 2005; Sanderson *et al.*, 2008]. Low values of the ice crystal fall speed were typically found in the ensemble members with a climate sensitivity at the higher end of the range. Furthermore, Mitchell *et al.* [2008] found the ice crystal fall velocity to have a significant importance for the cloud forcing. Jakob [2002] also found a dependence of the cloud forcing and the high cloud ice water path on the magnitude of the ice fall speed in the European Centre for Medium-Range Weather Forecasts model.

The work presented here is the first to investigate the climatic response from modifying cirrus clouds. An Earth System Model is used to investigate the possible impacts of deliberately modifying cirrus clouds, with a focus on Arctic sea ice and the hydrological cycle, in particular, the East Asian summer monsoon due to its great societal importance. The fall velocity of cloud ice is perturbed in a set of experiments, as an analogy to cloud seeding. The effects of changing the ice crystal fall speed on a hemispheric scale is also looked into. These sensitivity tests are a first step to evaluate the climatic effects and feasibility of this climate engineering option.

Section 2 describes the model and the experiment design. Section 3 presents the key findings from "seeding" globally, on hemispheric scales and outside of the tropics. Furthermore, results from an "overseeding" case [cf. Storelvmo *et al.*, 2013] are evaluated. Conclusions are drawn in section 4.

## 2. Method

### 2.1. The Model

The model used is the CESM (Community Earth System Model) version 1.0.3 [Hurrell *et al.*, 2013]. It couples four components together: atmosphere, land, sea ice, and ocean modules. The model is run at a latitude  $\times$  longitude resolution of  $0.9^\circ \times 1.25^\circ$ , with a time step of 20 min, and there are 30 vertical levels in the atmosphere. The atmospheric model, Community Atmosphere Model version 5.1 (CAM5.1), is a further development of CAM4, which is described in Gent *et al.* [2011] and Neale *et al.* [2013]. It uses a finite

volume dynamical core, and the cloud microphysics is improved compared to earlier versions [e.g., *Gettelman et al.* 2008, 2010]. The aerosol size distribution is represented by three lognormal modes (Modal Aerosol Model with three modes) [*Liu et al.*, 2011]. The radiation scheme has been updated to the rapid radiative transfer method, as per *Iacono et al.* [2008]. CAM5.1 simulates the interaction of aerosols and clouds, including cloud droplet activation, precipitation processes due to particle size, and the radiative interaction of cloud constituents.

The cirrus cloud microphysics scheme is after *Liu et al.* [2007] and includes heterogeneous immersion freezing of dust, which competes with homogeneous freezing of sulfate haze droplets. The freezing is dependent on the air temperature, updraft velocity, and aerosol properties. At temperatures below  $-40^{\circ}\text{C}$ , homogeneous freezing happens by instantaneous conversion of supercooled liquid water to cloud ice. Cloud ice is autoconverted to snow, depending on ice mass-weighted and number-weighted size distributions [*Ferrier*, 1994]. In the model, the size threshold where cloud ice is considered snow is  $400\ \mu\text{m}$  in diameter and the autoconversion time scale is 3 min. Aggregation of ice by snow follows *Lin et al.* [1983] and assumes that the ice crystal fall speed is much less than the snow fall speed. The particle fall speed differences between colliding hydrometeor species are accounted for. The fall speeds are scaled when different hydrometeors collide [*Ferrier*, 1994].

For mixed phase clouds, heterogeneous freezing occurs between  $-5$  and  $-35^{\circ}\text{C}$ . The immersion freezing of dust and black carbon follows *Diehl and Wurzler* [2004], while the contact freezing of dust is parametrized after *Liu et al.* [2007].

The land model is the Community Land Model version 4 described in *Oleson et al.* [2010] and *Lawrence et al.* [2011]. Glaciers, wetlands, vegetation, lakes, and urban surfaces are represented, and there are parametrizations for soils, river routing and runoff, carbon-nitrogen cycling, and a dust model [*Oleson et al.*, 2010]. The land cover and vegetation changes are dynamic.

The sea ice model is CICE4, i.e., the latest version of the Los Alamos Sea Ice Model [*Hunke and Lipscomb*, 2010]. It includes the thermodynamics of growth and melting of ice. Horizontal transport and mechanical redistribution is also accounted for. The sea ice model is coupled to the atmosphere and ocean components.

The oceanic model used in the experiment is a slab ocean model (SOM) version of the Parallel Ocean Program version 2 (POP2) model. It exchanges heat fluxes with the atmosphere and represents the mixed layer of the ocean. It aims to reproduce the coupled climate. SOM uses monthly mean fields, which are computed from a 20 yearlong simulation with the POP2 ocean model. Using a slab ocean in CESM has been shown to produce very similar results to using a full ocean circulation model by *Bitz et al.* [2011].

CAM5 has a higher climate sensitivity than its predecessor, CAM4 [*Gettelman et al.*, 2011]. The increase from 3.2 K to 4.0 K in the new model has been attributed to more positive cloud feedbacks and a higher radiative forcing from  $\text{CO}_2$  in CAM5. The water vapor path in CAM5 is within the observational range of the A-Train satellite estimates [*Jiang et al.*, 2012]. Compared to the Coupled Model Intercomparison Project Phase 5 models, CESM-CAM5 is within the upper range of both climate sensitivity and hence, not unexpectedly, water vapor path [*Gettelman et al.*, 2011; *Jiang et al.*, 2012]. This might affect the results of the experiments presented here, in that a high amount of upper tropospheric water vapor could increase the forcing potential of the engineering method discussed.

## 2.2. Experiment Design

The fall speed of an ice crystal in the microphysics scheme is represented by the following:

$$V = aD^b, \quad (1)$$

as per *Morrison and Gettelman* [2008], where  $V$  is the terminal ice crystal fall speed,  $D$  is the diameter of the ice particle, and  $a$  and  $b$  are constants with the values:  $a = 700\ \text{m}^{(1-b)}\ \text{s}^{-1}$  and  $b = 1$  [after *Ikawa and Saito*, 1990].

The fall speed was perturbed for all ice crystals, by either a doubling or halving, in the experiments. The doubling of the ice crystal fall speed is a coarse emulation of seeding with highly efficient ice nuclei and is here referred to as “seeding”, while reducing the fall speed mimics the “overseeding” regime described in *Storelvmo et al.* [2013].

**Table 1.** The Global Annual Mean Net Cloud Forcing (NCF) ( $W m^{-2}$ ), Ice Water Path (IWP), Liquid Water Path (LWP) ( $g m^{-2}$ ), Cloud Cover (CC) (%), and Net Shortwave and Longwave Fluxes at the Top of the Atmosphere (FSNT and FLNT, Respectively) ( $W m^{-2}$ ) From the Control Experiment and From Satellite Observations<sup>a</sup>

	NCF	IWP	LWP	CC	FSNT	FLNT
Observations	-23.8--17.2	20–70	30–50	71	238–242	236–243
Control	-26.2	15.5	44.0	62.5	239.4	238.6

<sup>a</sup>The cloud forcing and radiation data are from Clouds and the Earth's Radiant Energy System and Earth Radiation Budget Experiment, while the IWP, LWP, and cloud cover data are from CALIPSO and CloudSat [Jiang et al., 2012].

A suite of six model simulations were performed, one realization of each, as follows: (1) ct: control simulation, year 2000 time slice, (2) vfg: doubled ice crystal fall speed everywhere across the globe, (3) vfnH: doubled ice fall speed in the Northern Hemisphere, (4) vfSH: doubled ice fall speed in the Southern Hemisphere, (5) vf30: doubled ice fall speed in the extratropics (90–30°S and 30–90°N), and (6) vfgl: halved ice fall speed everywhere.

The simulations were run for 15 years, and the last 10 years were used in the analysis. Some key global annual mean fields from the control run and satellite observations are shown in Table 1.

The experiments are not realistic in the sense that the seeding is assumed to be at a uniform rate everywhere. This is not technically feasible in reality, and the seeding is more likely to happen at nonuniform rates on smaller scales. The tropospheric residence time of aerosols is of up to a couple of weeks. Therefore, the seeding would have to be almost perpetual as the seeding material keeps being depleted.

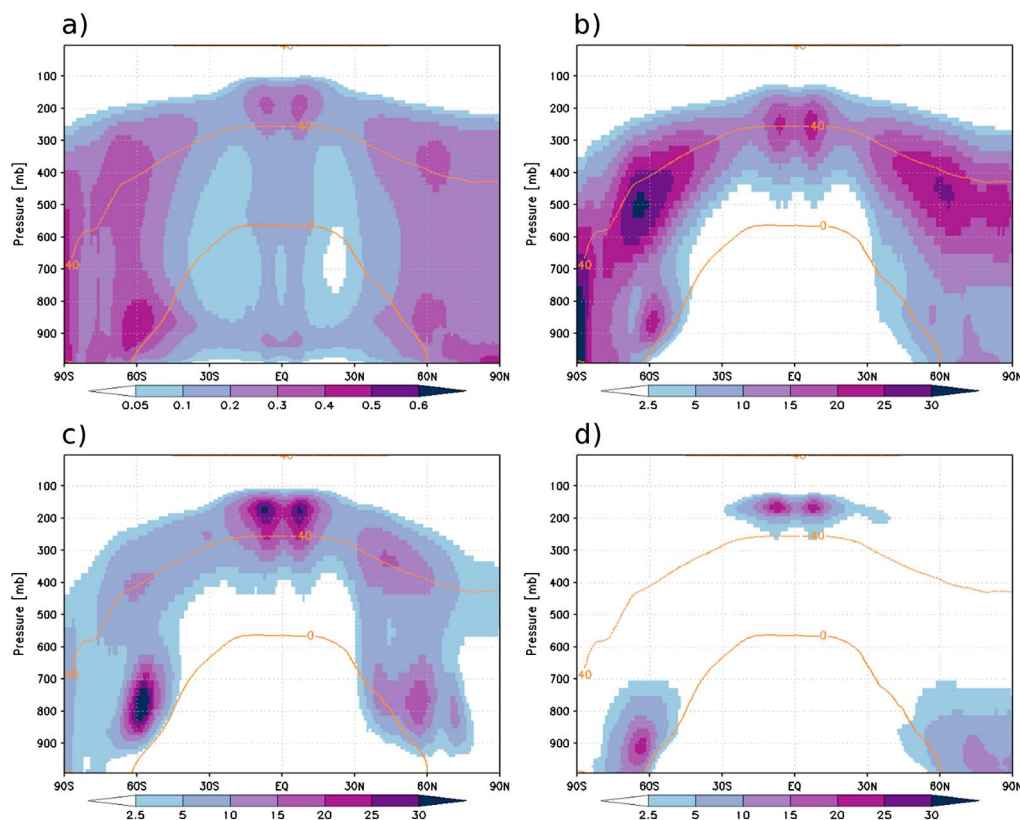


**Figure 1.** Annual mean control values: (a) fractional cloud cover, (b) ice crystal effective radius ( $\mu m$ ), (c) ice crystal number concentrations ( $l^{-1}$ ), and (d) the snow number concentrations ( $l^{-1}$ ). The 0 and  $-40^{\circ}C$  isotherms are shown in orange.

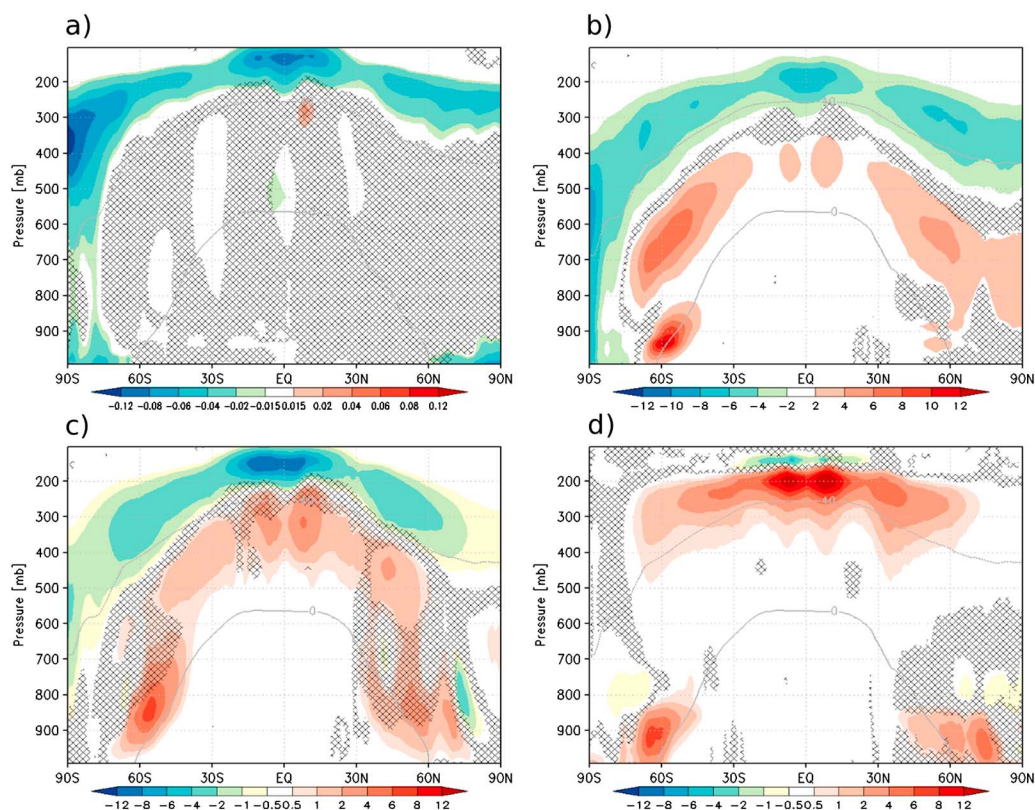


**Figure 2.** Annual mean differences between the vfg and ct experiments: (a) fractional cloud cover, (b) ice crystal effective radius ( $\mu\text{m}$ ), (c) ice crystal number concentrations ( $\text{l}^{-3}$ ), and (d) the snow number concentrations ( $\text{l}^{-3}$ ). The 0 and  $-40^\circ\text{C}$  isotherms are shown in gray. Nonhatching indicates a level of confidence higher than 95%.

Furthermore, the simple experiment design does not account for the full physical representation of all of the processes involved in cirrus cloud thinning. For example, there is no actual injection of ice nuclei in the upper troposphere, and hence neither any following activation nor growth into ice crystals. We simplify this by directly entering into the phase where the ice crystals have increased fall velocities. This is an oversimplification of the actual process but has the advantage of being repeatable as an experiment for other GCMs.

### 3. Results

This section presents some key findings from the experiments. First, the effects of increasing the ice crystal fall speed on a global scale are shown, including the changes to the cloud properties and key climatological variables. Then the hemispheric-scale experiments are presented, including the impacts on the hydrological cycle and Arctic sea ice, followed by the extratropical and “overseeding” scenarios. The statistical significance of the results was found using a Student’s *t* test with a *p* value of 0.05, and 1 year representing 1 degree of freedom. Figure 1 shows the zonal, annual mean cloud cover, effective radius of ice crystals, ice crystal number, and snow number concentrations from the control run, for reference to the anomaly plots in Figures 2, 8, 9, 11, and 13.

#### 3.1. The Effects of “Seeding” Globally

This section evaluates the results from the experiment where the ice crystal fall speed is doubled everywhere, i.e., the vfg experiment versus the ct, control run.

With regards to the cloud property changes (Figure 2), the ice crystal effective radius and number concentrations are reduced at high levels. As the ice crystals fall out of the high-level cirrus clouds, they collide with other crystals below aggregating into larger ice crystals and snow crystals. Therefore, more, larger crystals are seen below. As the large and heavy ice crystals fall downward, they are experiencing accretion of cloud ice by snow and accretion of cloud droplets onto snow and graupel, in addition to snow self-aggregation.

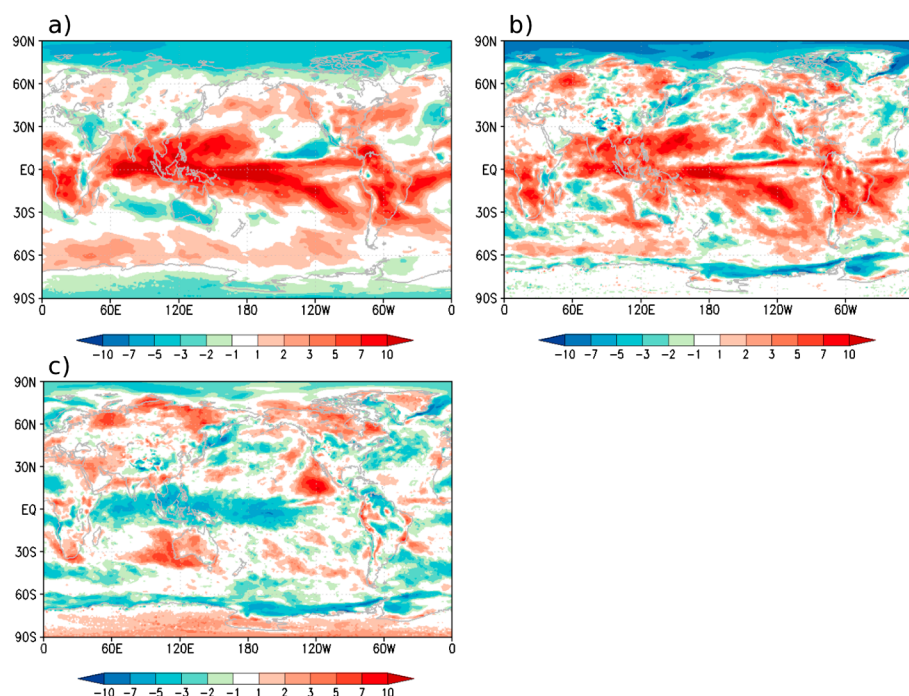


**Figure 3.** Annual mean TOA flux differences ( $\text{W m}^{-2}$ ) between the vfg and ct experiments: (a) net outgoing longwave (FLNT) global mean =  $1.57 \text{ W m}^{-2}$ , (b) net incoming shortwave (FSNT) global mean =  $1.06 \text{ W m}^{-2}$ , and (c) the net combined flux imbalance (FSNT-FLNT) global mean =  $-0.51 \text{ W m}^{-2}$ .

Aggregation has been shown to be an important ice particle growth mechanism [Mitchell *et al.*, 1996]. Crystals grow by colliding into each other and combining into larger “aggregates”. The process of size sorting, whereby large ice crystals fall more rapidly than smaller ones due to gravitation, results in an increased number of large crystals at lower levels, leaving the smaller ones at higher concentrations at upper cloud levels. The process of size sorting has been observed to be an important process in anvil cirrus clouds [Jensen *et al.*, 2009].

Clouds affect both the top of atmosphere (TOA) shortwave and longwave fluxes. The net energy imbalance at the TOA is the sum of all-sky shortwave and longwave fluxes, downward minus upward, and indicates if the climate is gaining or losing heat. Figure 3 shows the annual mean difference between vfg and ct in outgoing longwave flux at TOA (Figure 3a), net solar flux (Figure 3b), and the net radiation imbalance (FSNT-FLNT) (Figure 3c). The cirrus “seeding” results in increasing outgoing longwave radiation, particularly in the tropics and midlatitudes. The net TOA flux imbalance is  $-0.51 \text{ W m}^{-2}$ . The geographical distribution of the net flux imbalance shows a heat loss at low latitudes in particular, but also at high latitudes, due to feedbacks from clouds and sea ice. This pattern is different to the net fluxes from solar radiation management through a reduction in insolation, as identified in Schmidt *et al.* [2012, Figure 1]. These experiments are not directly comparable, though, as we are simply doubling the ice crystal fall speed and not seeking to offset a carbon dioxide quadrupling as such. The furthering of the Arctic amplification issue associated with solar radiation management is avoided with cirrus cloud thinning, due to the nature of the forcing. Targeting the longwave radiation instead of the shortwave as done with SRM, one avoids the inherent concern of Arctic residual warming [Kravitz *et al.*, 2013; Schmidt *et al.*, 2012]. Carbon dioxide has a relatively uniform distribution of radiative forcing, while incoming solar radiation is dependent on season and latitude, which is why Arctic thermal amplification is a crucial side effect of SRM. This can be avoided with cirrus cloud thinning climate engineering.

The reduction in coverage of the high, cold clouds (Figure 2a) allows more outgoing longwave (LW) radiation to escape the atmosphere. The increase in global annual mean outgoing longwave radiation is  $+1.57 \text{ W m}^{-2}$  in vfg (Figure 4). The global annual mean net cloud forcing change is of  $-1.55 \text{ W m}^{-2}$ , i.e., the change in longwave cloud forcing of  $-3.24 \text{ W m}^{-2}$  is about twice as large as the change in shortwave cloud forcing ( $+1.69 \text{ W m}^{-2}$ ). The reduction in the cirrus cloud albedo controls the SW (shortwave) cloud

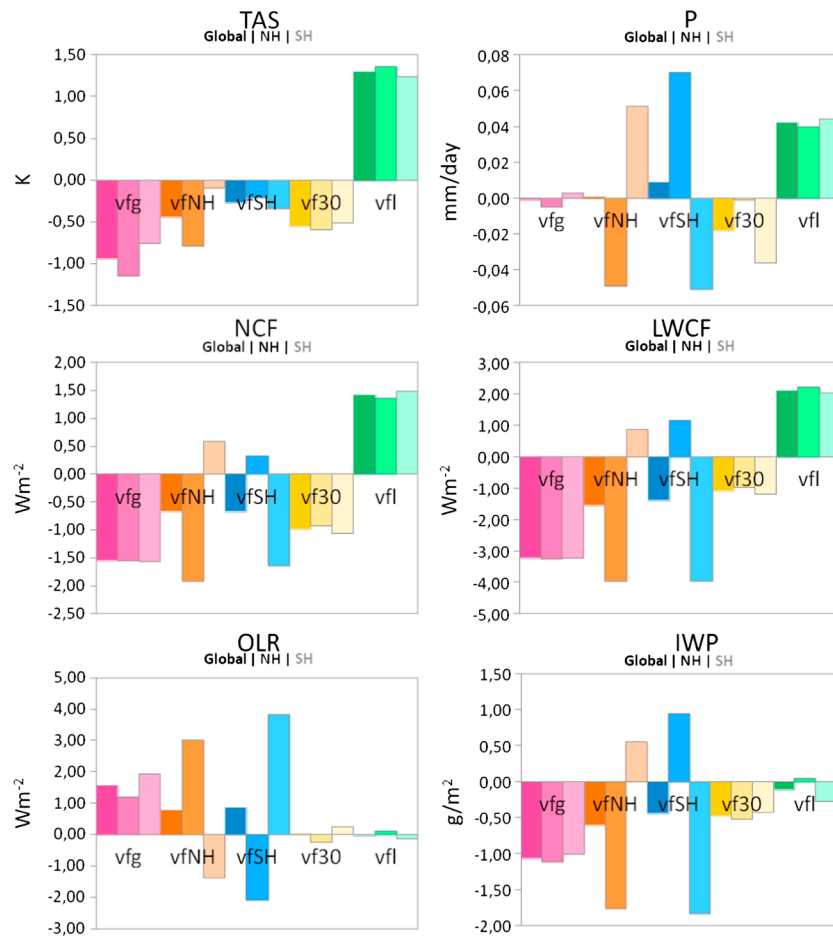


**Figure 4.** Area averages (global: darkest coloring, NH: medium coloring, and SH: lightest coloring) of annual mean differences from the control run: surface air temperature (TAS (K)), precipitation rate ( $P$  (mm/d)), net cloud forcing (NCF ( $W m^{-2}$ )), longwave cloud forcing (LWCF ( $W m^{-2}$ )), outgoing longwave radiation at the top of the atmosphere (OLR ( $W m^{-2}$ )), and ice water path (IWP ( $g/m^{-2}$ )). Magenta: vfg, orange: vfNH, blue: vfSH, yellow: vf30, and green: vfl.

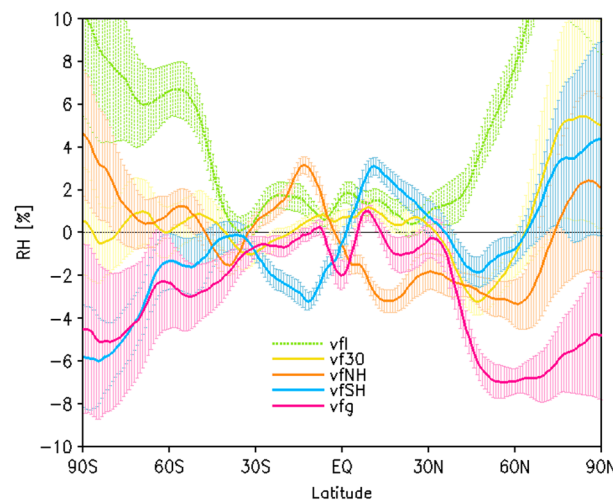


**Figure 5.** Annual zonal mean upper tropospheric relative humidity differences (%) from the control simulation. Green: vfl, yellow: vf30, orange: vfNH, blue: vfSH, and magenta: vfg. Error bars represent 1 standard deviation based on monthly means.

forcing. As the cirrus clouds are depleted, water vapor is removed in the upper troposphere (magenta curve in Figure 5). The reduction of this potent greenhouse gas contributes to the atmospheric cooling seen in the model (Figure 6a).

The results show a large-scale 2 m air temperature decrease, in the annual mean (Figure 6b) and through the seasons. The cooling extends through the whole troposphere, as seen in Figure 6a. The global annual mean change in surface air temperature is of  $-0.94 K$  (Figure 4), and there is a 3–4 K cooling in the Arctic (Figure 6b). The JJA Arctic temperature changes are  $-1-2 K$ , in conjunction with a sea ice fraction increase of 0.1–0.2 (Figure 6c).

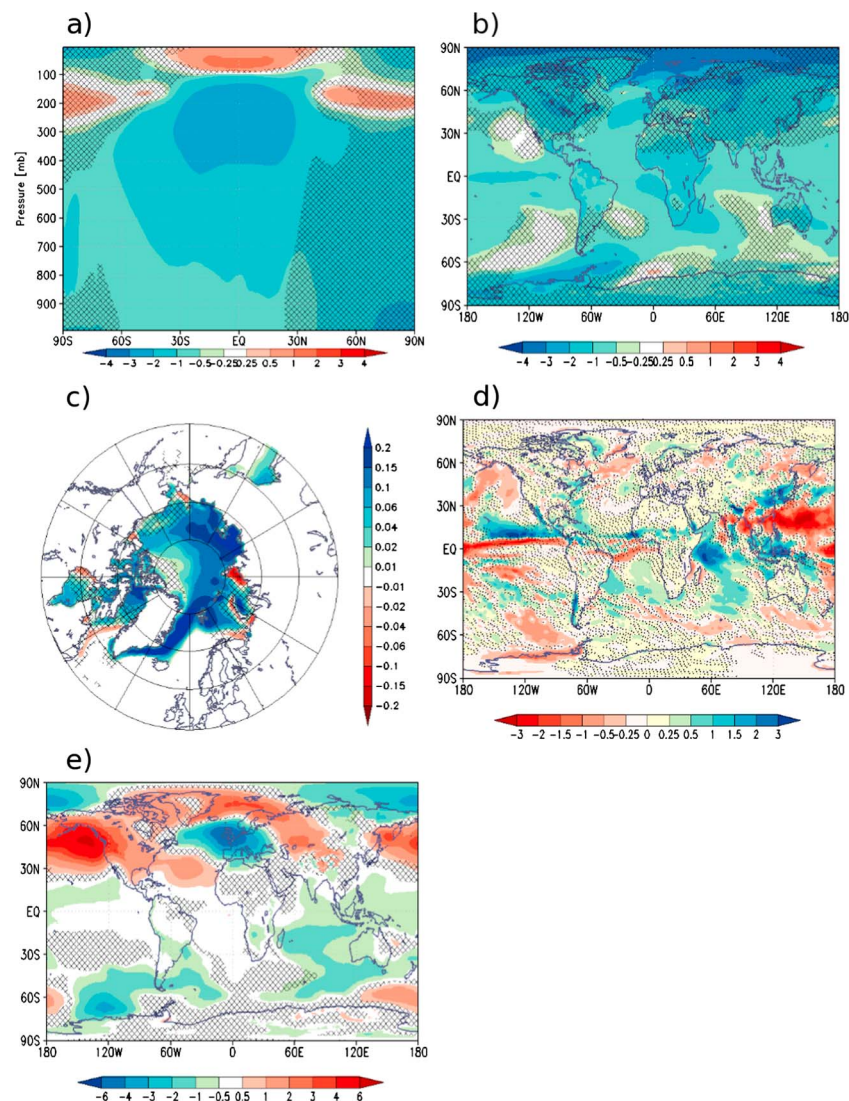


**Figure 6.** The differences between the vfg and ct experiments: (a) latitude versus height annual zonal mean temperature (K), (b) annual mean 2 m air temperature (K), (c) June, July, and August (JJA) sea ice fraction, (d) JJA precipitation-evaporation (mm/d), and (e) December, January, and February (DJF) sea level pressure (mb). Nonhatching indicates a level of confidence higher than 95%.

The global annual mean precipitation change is  $-0.001$  mm/d (Figure 4). Global cooling can hence be achieved while avoiding the reduction in global mean precipitation that is associated with SRM [Tilmes *et al.*, 2013]. The JJA precipitation-evaporation (P-E) (mm/d) changes are shown in Figure 6d. The JJA changes are shown due to our aforementioned interest in the NH monsoons. The largest changes are seen in the tropics, where the Pacific Walker Cell is stronger (Figure 7a). The Walker Index is defined as the difference in vertical velocity (Pa/s) positive  $\Omega$  values represent ascent) at the 500 mb level between the East Pacific ( $160^{\circ}\text{W}$ – $120^{\circ}\text{W}$ ) and West Pacific ( $120^{\circ}\text{E}$ – $160^{\circ}\text{E}$ ) between  $5^{\circ}\text{S}$  and  $5^{\circ}\text{N}$  [after Wang, 2005]. There is an increase in P-E in western tropical Pacific and a decrease in eastern parts of the Pacific. The east Pacific Hadley Index (the difference in vertical velocity at 500 mb between  $25^{\circ}\text{N}$ – $35^{\circ}\text{N}$ ,  $170^{\circ}\text{E}$ – $150^{\circ}\text{W}$  and  $5^{\circ}\text{S}$ – $5^{\circ}\text{N}$ ,  $160^{\circ}\text{W}$ – $120^{\circ}\text{W}$  [cf. Wang, 2005]) is weaker in JJA in vfg, while the west Pacific (difference in vertical velocity at 500 mb between  $25^{\circ}\text{N}$ – $35^{\circ}\text{N}$ ,  $110^{\circ}\text{E}$ – $150^{\circ}\text{E}$  and  $5^{\circ}\text{S}$ – $5^{\circ}\text{N}$ ,  $120^{\circ}\text{E}$ – $160^{\circ}\text{E}$ ) and Atlantic (difference in vertical velocity at 500 mb between  $20^{\circ}\text{N}$ – $30^{\circ}\text{N}$ ,  $90^{\circ}\text{W}$ – $70^{\circ}\text{W}$  and  $5^{\circ}\text{S}$ – $5^{\circ}\text{N}$ ,  $50^{\circ}\text{W}$ – $30^{\circ}\text{W}$ ) Hadley Indices are only slightly stronger (Figure 7b). Across the Sahel, P-E is increased by 0.25–1.5 mm/d.

There is a strengthening of the northwest Pacific subtropical high by 3 mb. This pressure cell is known to be a key modulator of the East Asian summer monsoon [e.g., Chang *et al.*, 2000; Wang *et al.*, 2000; Lee *et al.*,



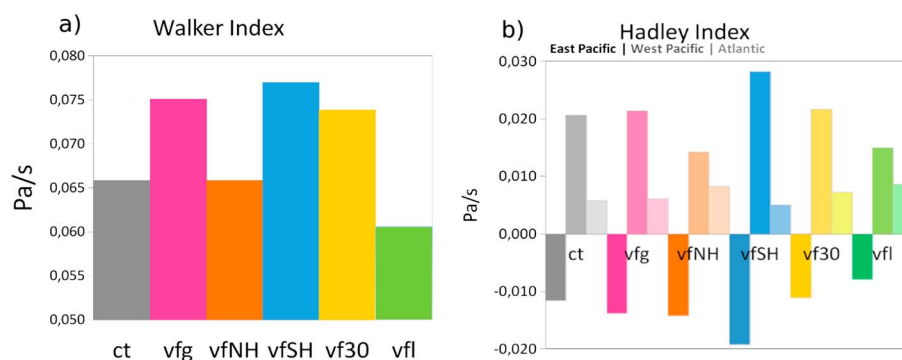


**Figure 7.** (a) JJA Pacific Walker Index. (b) JJA Hadley Indices, where darker coloring indicate East Pacific Hadley Index, medium coloring show the West Pacific Hadley Index, while the lightest coloring show the Atlantic Hadley Index. Grey: ct, magenta: vfg, orange: vfNH, blue: vfSH, yellow: vf30, and green: vfl.

2005, 2006]. The expansion and strengthening of this high pressure cell lead to an intensification over land of the East Asian summer monsoon (EASM). The changes to the high deepen and shift the monsoon front onshore. The EASM feeds on the moist advection from the high. There is a high pressure anomaly in the Bay of Bengal suppressing the Indian Monsoon precipitation.

The warming of the stratosphere in the tropics, in particular, and NH midlatitudes (Figure 6a) is due to more longwave radiation from the surface and the lower troposphere reaching these high levels in the atmosphere. Since the LW-trapping cirrus have been depleted, more of the outgoing LW radiation reaches the stratosphere where  $\text{CO}_2$  and  $\text{O}_3$  absorb more radiation; hence, a warming is seen. Dynamically, as the troposphere is cooling down and the air is compressing, the tropopause height is being lowered. This in turn facilitates an expansion and warming of the stratosphere. The warming of the stratospheric temperatures is in association with a weaker wintertime polar vortex and a weaker jet stream. The jet stream becomes more sluggish and meandering, allowing for break outs of pockets Arctic air. Weaker vortex conditions, with anomalous warm stratospheric temperatures are typical of Arctic Oscillation in a negative phase [Thompson and Wallace 1998]. Weak vortex conditions have a tendency to propagate downward and affect the troposphere [Black, 2002; Tomassini et al., 2012]. The cold point tropopause (the coldest point in the temperature profile) over the Arctic is 200–300 m lower in vfg than in the control simulation. This contributes to a compression of the underlying troposphere, enabling anticyclonic activity. The anomalous high pressure (Figure 6e) and cold DJF temperatures over North America and northern Europe/Eurasia allow for the outflow of cold Arctic air, acting as a positive feedback amplifying the cold DJF temperature anomalies over the northern continents (not shown). The higher pressure over the Arctic is a result of the cooling from the cirrus cloud thinning, in combination with the circulation changes induced from stratospheric vortex anomalies.

### 3.2. Hemispheric-Scale “Seeding”

Simulations were performed in which the ice crystal fall speed was doubled in the Northern and the Southern Hemispheres separately. “Seeding” the NH or SH only results in the same type of response in the cloud properties as on a global scale (Figures 8 and 9). Fewer and smaller ice crystals are seen at high levels, with more numerous and larger ice crystals below in the “seeded” hemisphere. Additionally, there is an increase in the ice crystal number concentration in the tropics of the “nonseeded” hemisphere (size sorting). This could be due to the temperature asymmetry of the hemispheres and the Intertropical Convergence Zone (ITCZ) preferring residence in the “nonseeded”, warmer one—a feature also found by Haywood et al. [2013] using hemispheric-scale stratospheric sulfur injections. A southward (northward) ITCZ shift is seen in JJA in vfNH (vfSH) (Figures 10a and 10b), though less coherently so in vfNH than vfSH. By “seeding” and therefore cooling the SH in vfSH, the NH summer monsoons are shifted further north and onto land, increasing P-E over northwestern Africa, Central America, and the EASM region with a magnitude of 0.25–1.5 mm/d. Haywood et al. [2013] also found that cooling the SH via climate engineering resulted in an increase in the Sahelian summer precipitation, consistent with our results.

The northwest Pacific subtropical high is strengthened by 1–2 mb in JJA in both vfNH and vfSH. This contributes to the onshore push of the monsoon front. The subtropical high is stronger due to the combined changes to the Hadley and Walker circulations. The anomalous high blocks the Meiyu front from retreating

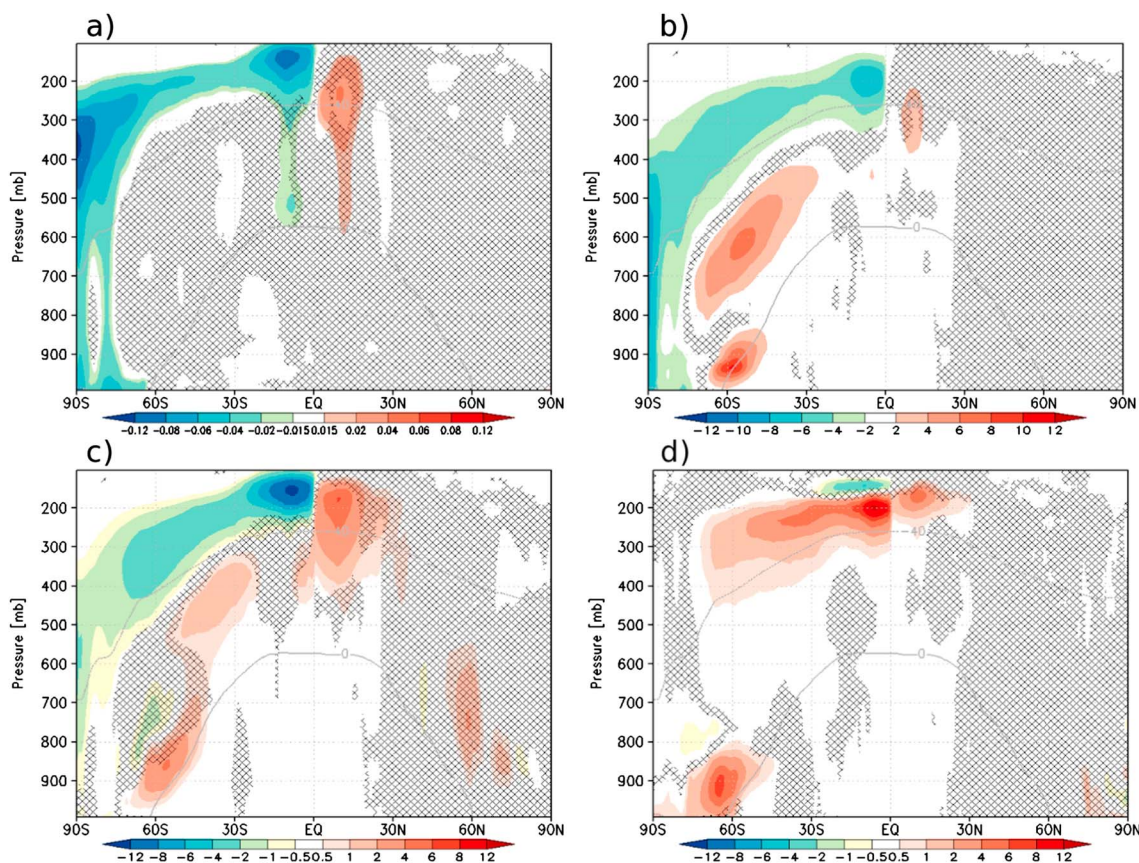


**Figure 8.** Annual mean differences between the vfSH and ct experiments: (a) fractional cloud cover, (b) ice crystal effective radius ( $\mu\text{m}$ ), (c) ice crystal number concentrations ( $\text{l}^{-1}$ ), and (d) the snow number concentrations ( $\text{l}^{-1}$ ). Nonhatching indicates a level of confidence higher than 95%.

southward, and hence, more of the monsoon rain falls over land, rather than the ocean [Lee *et al.*, 2013]. The stronger high pressure offers another positive feedback as it also sharpens the pressure gradient to the west-northwest, reintensifying the East Asian monsoon front [Chen, 1983]. The Pacific Walker Circulation is intensified in vfSH, while its intensity is unchanged in vfNH, as indicated in Figure 7a.

When “seeding” the NH only, the hemispheric temperature relationship is reversed and the asymmetry between the hemispheres is reduced. There is a 0.79 K cooling of the NH in the annual mean in vfNH, while the SH cools by 0.09 K (Figure 4). In the vfSH experiment on the other hand, the SH cools only slightly more than the NH (0.34 K cooling in SH and 0.21 K in the NH). The fall speed perturbations in vfNH and vfSH lead to a cooling extending vertically to the tropopause in the “seeded” hemisphere. “Seeding” the NH leads to a stronger cooling than “seeding” the SH (Figure 4). This is due to the NH having a larger land mass than the SH, and the land warms quicker than the ocean. The stronger cooling in NH could also be partly due to the higher concentration of ice crystals in this hemisphere in the model; hence, there is a larger cooling potential with this climate engineering technique in the NH.

There are some compensating effects in the “nonseeded” hemisphere, as seen in Figure 4. For instance, there is an increase in the ice water path, upper tropospheric relative humidity (Figure 5), and longwave cloud forcing in the SH (NH) in vfNH (vfSH), due to the shifts in the ITCZ. The “seeded” hemisphere changes, however, are larger, and the global net effects are of the desired sign. There is a reduction in the annual mean upper tropospheric (200–300 mb) relative humidity in the “seeded” hemisphere (Figure 5).

In both vfSH and vfNH, the tropical stratosphere is warmer, while the Arctic stratosphere is much colder in DJF. This enhanced meridional gradient strengthens the north polar vortex and the jet stream. The stronger jet stream favors positive North Atlantic Oscillation (NAO) tendencies in the experiments.

In vfNH there is a cooling of the near surface air temperatures of 1–2 K in JJA in much of the NH, accompanied by an increase in the Arctic JJA sea ice fraction (Figure 10d). In vfSH, the NH cools by 0.21 K in JJA, and

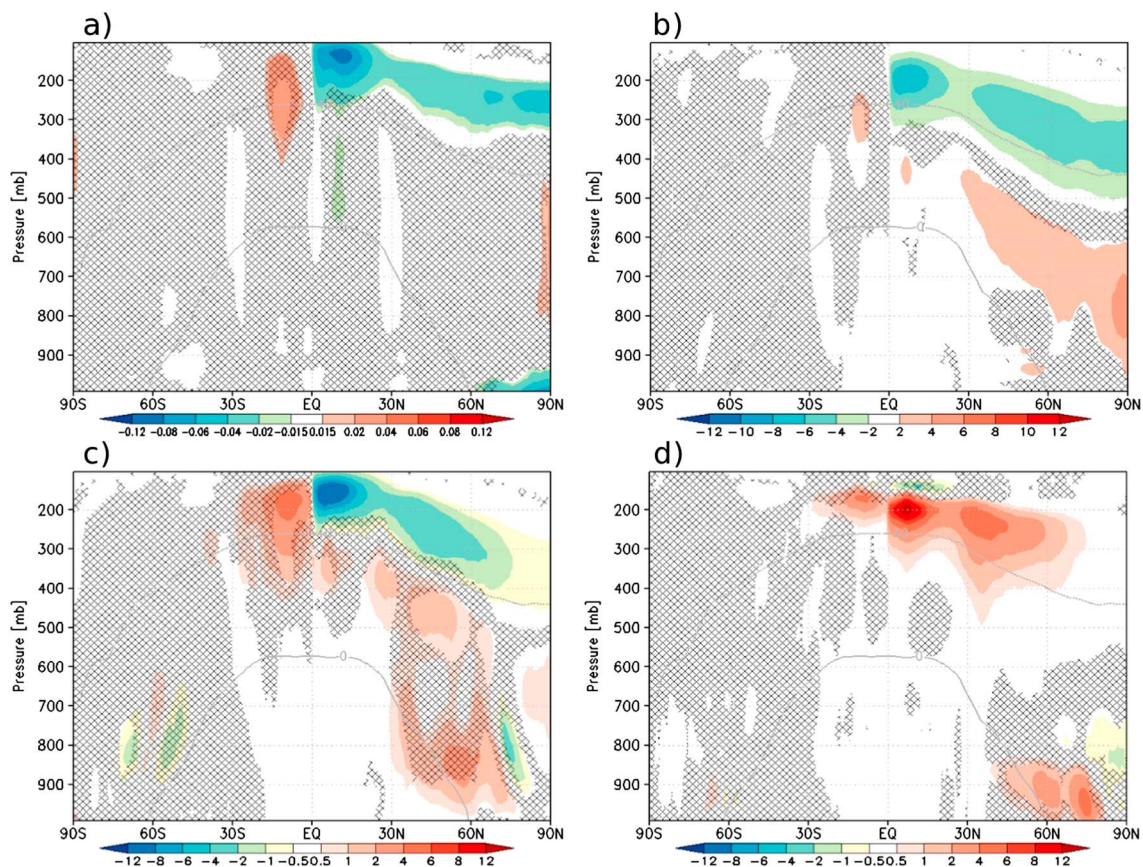


**Figure 9.** Annual mean differences between the vfNH and ct experiments: (a) fractional cloud cover, (b) ice crystal effective radius ( $\mu\text{m}$ ), (c) ice crystal number concentrations ( $\text{l}^{-1}$ ), and (d) the snow number concentrations ( $\text{l}^{-1}$ ). Nonhatching indicates a level of confidence higher than 95%.

there is an increase in the JJA sea ice in the Arctic; however, it is confined to the East Siberian Sea. The Beaufort Sea, on the other hand, sees a reduction of 0.15 (Figure 10c). This reduction is due to the anomalous southerly winds in the Bering Sea bringing warm marine air in from the Pacific (Figure 10e). This anomalous air flow originates from the high pressure anomaly over the North Pacific, stretching from Okhotsk to the Aleutian archipelago. This high is due to anomalous jet structures resulting from the dynamic response to the temperature changes from the “seeding”.

In vfSH the wintertime Siberian high is strengthened by up to 2 mb (not shown, but statistically significant at the 95% level). This results in a further isolation of the air masses within the center of the high and an enhanced cooling and increase in snow cover. This positive snow cover anomaly persists though springtime and permits the cooling signal to impact the summer climate.

### 3.3. “Seeding” Outside the Tropics

One simulation was performed to evaluate the effects of “seeding” everywhere external to the tropics, which we defined as  $\pm 30^\circ$  latitude. The motivation for this experiment is that tropical cirrus clouds are typically associated with anvils in towering cumulonimbus clouds. Anvils contain the out-flowing air from the deep convection where the low-level air has ascended through the cloud and into the anvil. As explained in Mitchell *et al.* [2011], seeding tropical anvil cirrus would not be a straightforward exercise due to strong updrafts. Anvil ice crystals typically form and grow in these strong updrafts.

In the vf30 simulation, relative to the control simulation, there is a reduction in the ice water path outside of the tropics, especially at high latitudes. Figure 11a shows the thinning of high clouds. This is accompanied by a reduction in the longwave cloud forcing of  $1\text{--}6 \text{ W m}^{-2}$  almost everywhere outside of the tropics.

A cooling of  $0.55^\circ\text{C}$  is seen in the global annual mean (Figure 4). There is a cooling mostly everywhere throughout the seasons (not shown). Due to the cooler temperatures, there is a JJA increase in the sea ice fraction across the Arctic of  $0.1\text{--}0.2$  (not shown).

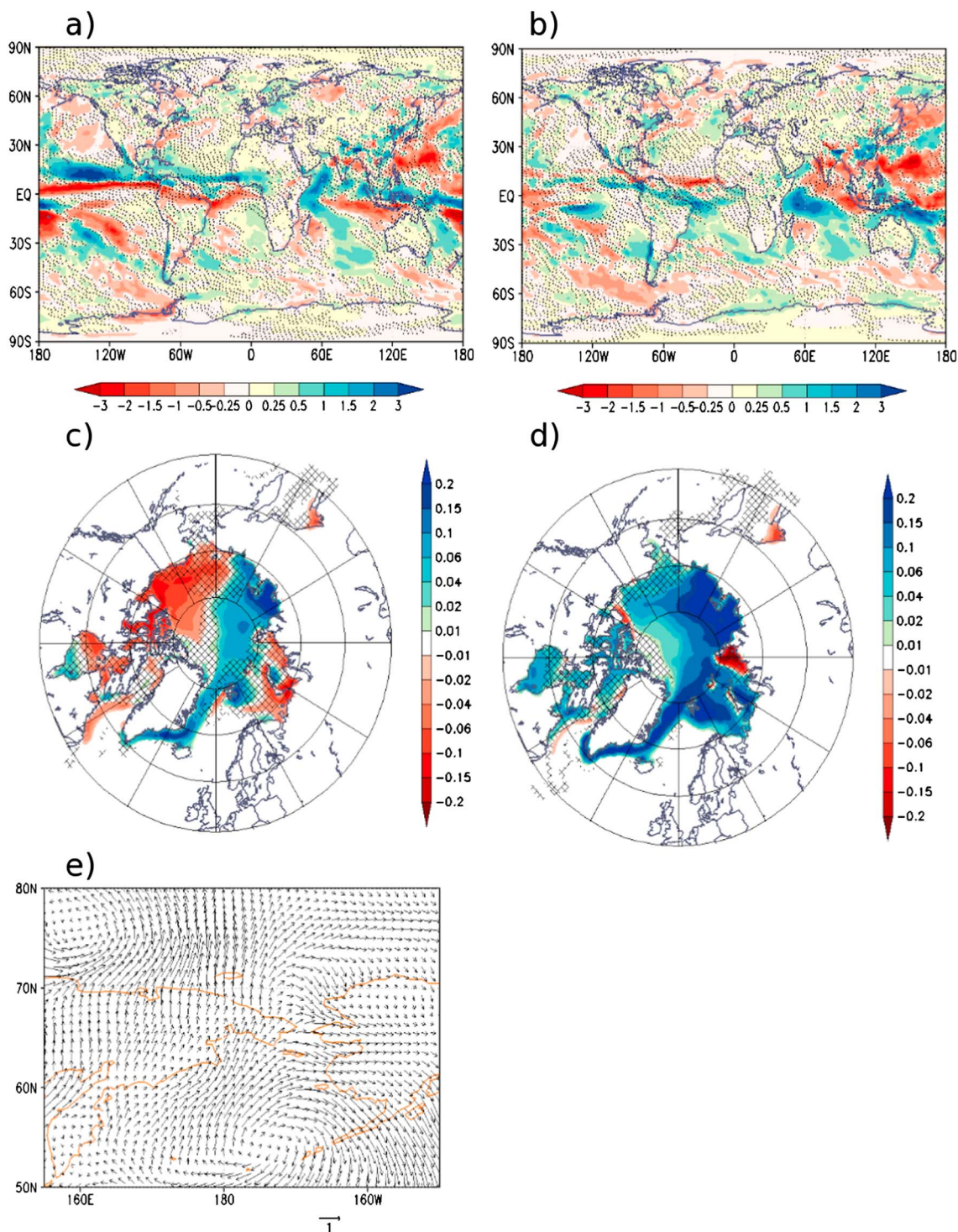


**Figure 10.** JJA P-E differences from the control: (a) vfSH and (b) vfNH. JJA sea ice fraction differences from control: (c) vfSH and (d) vfNH. (e) The JJA surface wind differences between vfSH and the control (m/s). Nonhatching indicates a level of confidence higher than 95%.

As the cirrus clouds are depleted and a cooling ensues, the tropical stratosphere warms, as the tropopause height is lowered by 50–300 m. The DJF warming of the tropical stratosphere and cooling of the Arctic stratosphere (Figure 12a) increases the meridional pressure gradient in the upper troposphere-lower stratosphere. This in turn sets up a stronger polar vortex. A strong Arctic vortex enhances the jet stream, which is often a precursor to positive North Atlantic Oscillation conditions [Baldwin, 2000]. There are signs of

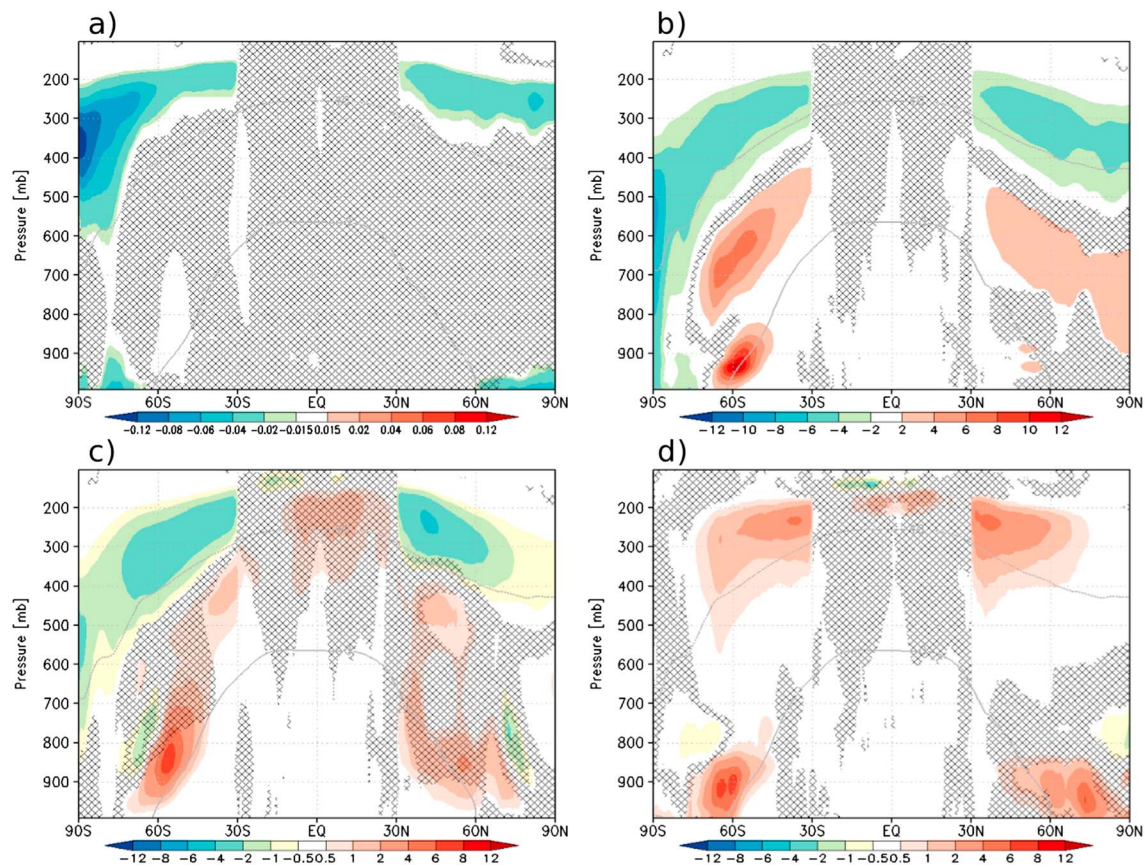


**Figure 11.** Annual mean differences between the vf30 and ct experiments: (a) fractional cloud cover, (b) ice crystal effective radius ( $\mu\text{m}$ ), (c) ice crystal number concentrations ( $\text{l}^{-1}$ ), and (d) the snow number concentrations ( $\text{l}^{-1}$ ). Nonhatching indicates a level of confidence higher than 95%.

positive NAO-like features during DJF in the model, with high pressure anomaly over the Azores and a negative one in the North Atlantic, centered NW of the British Isles (Figure 12b). The increase in the pressure gradient strengthens the westerlies resulting in a wetter winter across much of Europe (Figure 12c). These pressure anomalies also cause positive surface temperature anomalies over subtropical North Atlantic and southern Europe (not shown), counteracting the intention of the climate engineering.

Arctic amplification, the stronger warming at NH high latitudes compared to midlatitudes, is not only an issue of global warming [Screen and Simmonds, 2010], but also a caveat of Solar Radiation Management [Kravitz et al., 2013; Schmidt et al., 2012]. The slowing down of the NH jet stream and meridional Rossby waves, with increased amplitudes, have been linked to the amplification of the anthropogenic warming in the Arctic [Francis and Vavrus, 2012]. The slower upper level Rossby waves allow for the development of persistent midlatitudinal weather patterns, increasing the likelihood of the occurrence and magnitude of extreme events [Francis and Vavrus, 2012]. The vf30 results suggest that the Arctic amplification issue could possibly be counteracted via cirrus cloud thinning. As the meridional temperature gradient is increased at NH high levels, the jet stream is strengthened and the Arctic is cooler than the control run. A stronger jet stream prevents the occurrence of blocking highs. Hence, the influence of Arctic amplification on extreme weather events could be reduced through this method.

The largest JJA precipitation-evaporation changes are located in the West Pacific, where the northwest Pacific subtropical high is anomalously strong. This, coupled to an Okhotskian pressure anomaly, affects the summer monsoon in the area. The Okhotsk High is known to regulate the Asian monsoon fronts [e.g., Ninomiya and Mizuno, 1985; Ninomiya, 1987; Wang, 1992; Muri et al., 2012] and can also be associated with the NAO [Ogi et al., 2003; Ogi et al., 2004]. These pressure anomalies squeeze the EASM front, in the sense that the high ensures a longer rainy season over land, inhibiting the southeastward end-of-season retreat. At the same time, the high anomaly strengthens the equatorial trade winds in the western Pacific, reinforcing the precipitation there (Figure 12d). There is a strengthening of the JJA Pacific Walker Circulation

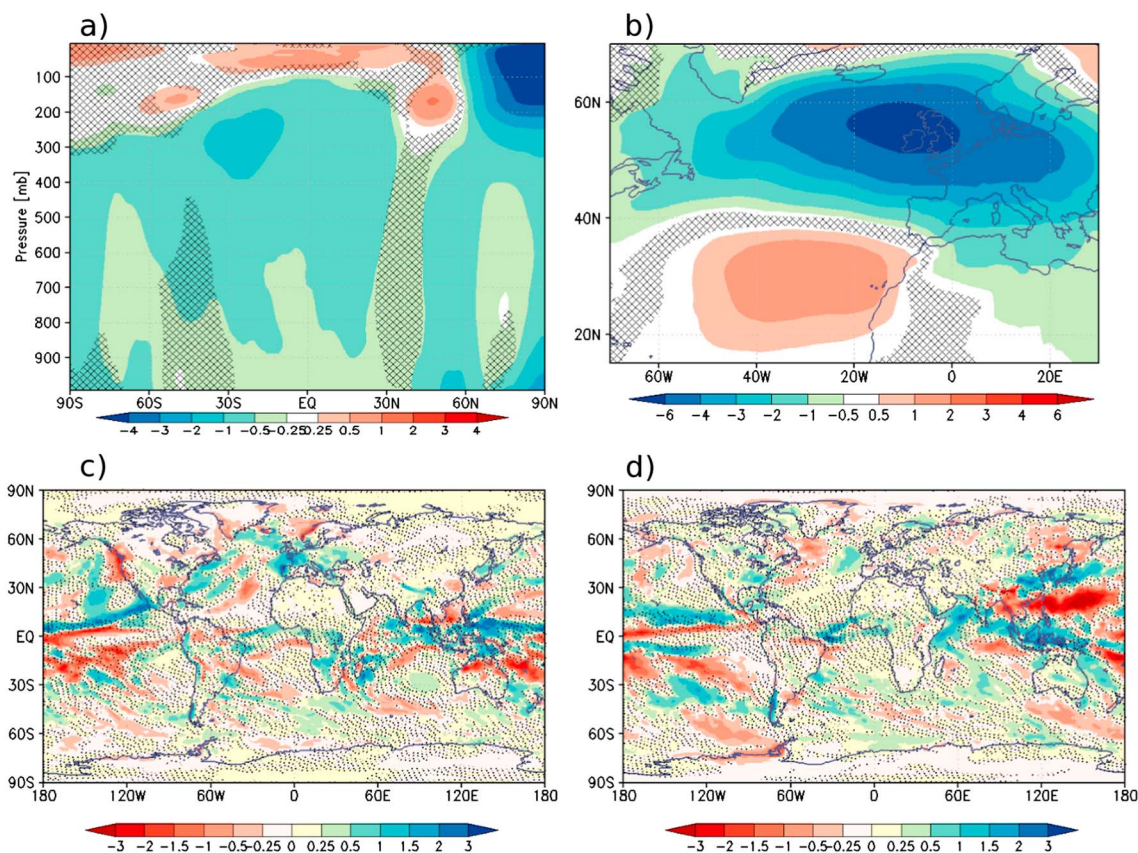


**Figure 12.** Differences between vf30 and control: (a) zonal DJF mean temperatures (K), (b) North Atlantic DJF mean sea level pressure (mb), (c) DJF P-E, and (d) JJA P-E (mm/d). Nonhatching indicates a level of confidence higher than 95%.

(Figure 7a), which is indicated by an increase in P-E over the Maritime Continent and a decrease in eastern Pacific. The JJA surface cooling at higher latitudes reinforces the meridional temperature gradient, affecting the Hadley Circulation. The Atlantic and west Pacific Hadley Indices are slightly higher in vf30 than the control run (Figure 7b). These results underline the risk of climatological changes occurring remotely of climate engineered regions.

### 3.4. An Analogy to Overseeding

The experiment where the ice crystal fall speed was halved, vfgl, can be seen as an analogy to overseeding the cirrus clouds. If too many ice nuclei are introduced to the cirrus-forming regions, homogeneous nucleation is not only suppressed, but a very high number of small ice crystals would form. Hence, the seeded cirrus clouds would consist of more numerous and smaller ice crystals than the unseeded clouds, leading to not only a higher cloud albedo but also more trapped longwave radiation, as explained in *Storelvmo et al.* [2013]. This is illustrated in Figure 13, showing an increase in high cloud cover and ice crystal numbers.

The results from this experiment show a global annual mean tropospheric warming of 1–2 K near the surface (Figure 14a). The global annual mean net cloud forcing change is of  $+1.4 \text{ W m}^{-2}$  (Figure 4). The Arctic DJF temperatures are as much as 5 K higher than in the control (Figure 14b) and the sea ice edge retreats several degrees northwards. The JJA sea ice fraction is reduced by 0.15–0.20 across the Arctic Ocean (Figure 14c). The warmer vfgl climate has a reduction of both the Walker and Hadley Indices (Figure 7) compared to the control simulation, consistent with *Lu et al.* [2007]. This experiment indicates the potential dangers of overseeding cirrus clouds, should society choose to implement this method of climate engineering.

Parallels can be drawn between contrails and “overseeding”. Aircraft emissions of aerosols and aerosol precursors can lead to changes to and formation of clouds, e.g., contrails [*Intergovernmental Panel on Climate Change (IPCC)*, 1999]. Condensation trail formation depends on the background meteorological state of the flight track, including temperature and humidity. The net radiative forcing effect is very uncertain but has

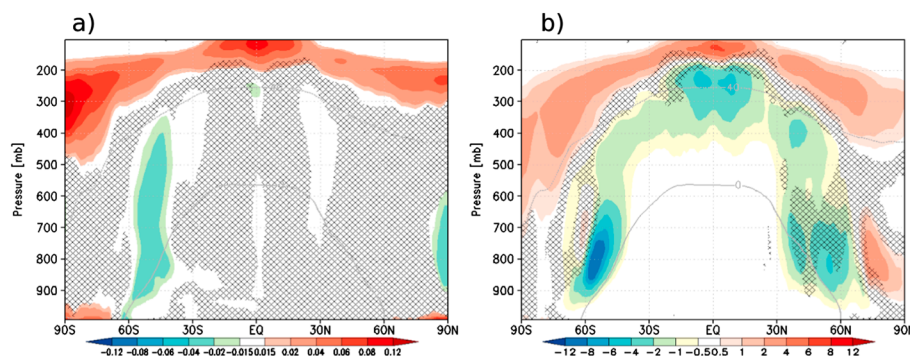


**Figure 13.** Annual mean differences between the vfl and ct experiments: (a) fractional cloud cover and (b) ice crystal number concentrations ( $l^{-1}$ ). Nonhatching indicates a level of confidence higher than 95%.

been estimated to be positive but small, on the order of  $+0.01 W m^{-2}$  [Sausen et al., 2005]. Parallels can be drawn between contrail cirrus (due to shearing and spreading of line contrails [Minnis et al., 1998]) formation from commercial aviation and “overseeding” of cirrus clouds. Contrails will continue to grow and can develop into contrail cirrus clouds, when the ambient air is supersaturated with respect to ice.

According to in situ observations, contrails are dominated by a high concentration of small, pseudospherical ice crystals [Schröder et al., 2000]. The exhaust consists of black carbon soot and liquid volatile aerosols, including sulfate [IPCC, 1999]. The ice crystal number concentrations in fresh contrails are typically as high as a few  $1000 cm^{-3}$  with an effective radius of  $1.5-10 \mu m$  [Schröder et al., 2000]. The “overseeding” scenario of Storelvmø et al. [2013] show a positive cloud forcing for such small particles in these very high concentrations. There might be valuable information in the literature on contrail cirrus and with the parallels to the “overseeding” regime of Storelvmø et al. [2013]; this should be further investigated in the future. Furthermore, investigation of cirrus cloud thinning in climate models can even inform the discussion on contrails, considering aviation exhausts have been increasing over the past decades and are expected to continue to increase in the future. Hence, investigation of “overseeding” in models could shed light on the effects of future commercial air traffic increase.

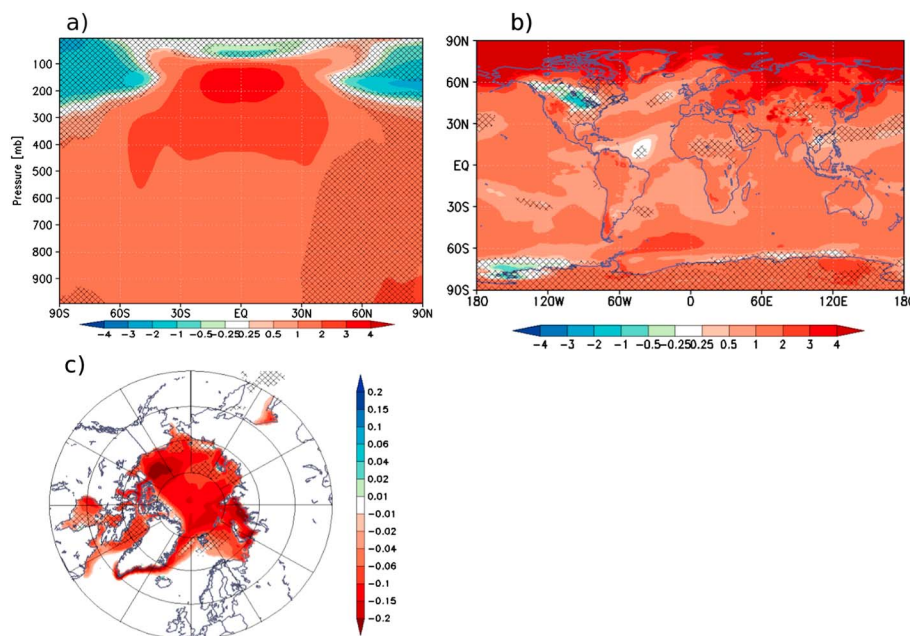


**Figure 14.** Annual mean differences between the vfl and ct experiments: (a) annual mean temperature, (b) DJF temperature (K), and (c) JJA Arctic sea ice fraction. Nonhatching indicates a level of confidence higher than 95%.

#### 4. Conclusions

A set of simple sensitivity tests perturbing the ice crystal fall speed in CESM were performed in order to assess possible climatic responses to climate engineering via cirrus cloud thinning. These simple experiments highlight the cooling potential of this climate engineering method. Research into radiation management in the form of cirrus cloud thinning should be given consideration alongside the other proposed climate engineering methods. A change in the net cloud forcing of  $-1.55 \text{ W m}^{-2}$  was found by doubling the ice crystal fall speed everywhere. A cooling of about  $1^\circ\text{C}$  in the annual mean was obtained from “seeding” globally. Arctic summer sea ice conditions were overall alleviated in the experiments, though “seeding” in the Southern Hemisphere only caused a decrease in JJA Arctic sea ice from the resulting atmospheric circulation changes. The global annual mean change in precipitation-evaporation was found to be small in the experiments, but large regional and seasonal changes, including changes to the monsoons, resulted from the climate engineering.

Reducing the optical depth and lifetime of cirrus clouds, thus reducing the longwave radiation trapping, does not tackle the underlying issue of global warming: anthropogenic greenhouse gas emissions. It does, however, target the relevant part of the radiation budget (i.e., LW), as opposed to climate engineering options directed at the shortwave radiation, such as stratospheric sulfur injections and marine cloud brightening. Additionally, cirrus cloud thinning targets upper tropospheric water vapor, which was found to be reduced in the “seeded” areas in these experiments.

Cooling the Southern Hemisphere only via climate engineering, and hence increasing the hemispheric temperature asymmetry, could alleviate Sahelian drought conditions. Targeting the Northern Hemisphere only gave a stronger cooling than when the Southern Hemisphere was engineered, due to the differences in land-sea distribution between the hemispheres. The hemispheric-scale experiments showed some compensational effects in the “nonseeded” hemisphere. “Seeding” outside of the tropics only resulted in climatological changes in the “nonseeded” regions, including changes in the East Asian summer monsoon.

The ice water path in the control simulation is too low compared to the satellite observations, which is a common issue with models [Eliasson *et al.*, 2011]. The IWP is important in determining the radiative properties of the clouds in the radiation scheme in models. Too little high level ice in the model could mean that the magnitude of the response to the “seeding” is on the low side.

As opposed to solar radiation management approaches, which are based on reflecting more incoming solar radiation, cirrus cloud thinning manages to cool global temperatures, without reducing global annual mean precipitation rates. Furthermore, the issue of Arctic amplification of temperatures inherent to SRM is avoided though this climate engineering technique.

The presented results conceptualize how cloud modifications can lead to changes in the radiation, then temperatures, and furthermore changes to the dynamics and atmospheric circulation, thus underpinning the risk of inducing undesirable consequences remote of the climate engineered region. Cooling might be achieved, but on the flip side unwelcome side effects on the climate, such as changes in the hydrological cycle and atmospheric circulation changes, could ensue. The climate system is complex and highly nonlinear in its behavior, and perturbing one element of it can lead to unforeseen changes; climate engineering should therefore be approached with great caution.

The study presented here should not be seen as advocacy for climate engineering. Scientific information is, however, an essential component of the climate engineering debate.

#### Acknowledgments

This work is supported by the EU 7th Framework Programme grant agreement 306395, EuTRACE, and the Norwegian Research Council projects EarthClim (207711/E10) and EXPECT (229760/E10). Norwegian Research Council's Program for supercomputing, NOTUR, provided the computing time. We are grateful for the constructive comments from the reviewers.

#### References

- Baldwin, M. (2000), The Arctic Oscillation and its role in stratosphere-troposphere coupling, *SPARC News Lett.*, *14*, 10–14.
- Bitz, C. M., K. M. Shell, P. R. Gent, D. A. Bailey, G. Danabasoglu, K. C. Armour, M. M. Holland, and J. T. Kiehl (2011), Climate sensitivity of the Community Climate System Model, version 4, *J. Clim.*, *25*(9), 3053–3070, doi:10.1175/jcli-d-11-00290.1.
- Black, R. X. (2002), Stratospheric forcing of surface climate in the Arctic Oscillation, *J. Clim.*, *15*, 268–277.
- Bower, K., T. Choulaton, J. Latham, J. Sahaee, and S. Salter (2006), Computational assessment of a proposed technique for global warming mitigation via albedo-enhancement of marine stratocumulus clouds, *Atmos. Res.*, *82*(1–2), 328–336, doi:10.1016/j.atmosres.2005.11.013.
- Chang, C. P., Y. Zhang, and T. Li (2000), Interannual and interdecadal variation of the East Asian summer monsoon and tropical Pacific SSTs. Part 1: Roles of the subtropical ridge, *J. Clim.*, *13*, 4310–4325.
- Chen, G. T. J. (1983), Observational aspects of the Mei-Yu phenomena in subtropical China, *J. Meteorol. Soc. Jpn.*, *61*, 306–312.



- Crutzen, P. J. (2006), Albedo enhancement by stratospheric sulphur injections: A contribution to resolve a policy dilemma?, *Clim. Change*, 77, 211–220.
- Cziczo, D. J., K. D. Froyd, C. Hoose, E. J. Jensen, M. Diao, M. A. Zondlo, J. B. Smith, C. H. Twohy, and D. M. Murphy (2013), Clarifying the dominant sources and mechanisms of cirrus cloud formation, *Science*, 340(6138), 1320–1324, doi:10.1126/science.1234145.
- Diehl, K., and S. Wurzler (2004), Heterogeneous drop freezing in the immersion mode: Model calculations considering soluble and insoluble particles in the drops, *J. Atmos. Sci.*, 61(16), 2063–2072, doi:10.1175/1520-0469(2004)061<2063:HDFITI>2.0.CO;2.
- Eliasson, S., S. A. Buehler, M. Milz, P. Eriksson, and V. O. John (2011), Assessing observed and modelled spatial distributions of ice water path using satellite data, *Atmos. Chem. Phys.*, 11, 375–391.
- Ferrier, B. F. (1994), A double-moment multiple-phase four-class bulk ice scheme. Part I: Description, *J. Atmos. Sci.*, 51, 249–280.
- Francis, J. A., and S. J. Vavrus (2012), Evidence linking Arctic amplification to extreme weather in mid-latitudes, *Geophys. Res. Lett.*, 39, L06801, doi:10.1029/2012GL051000.
- Gent, P. R., et al. (2011), The Community Climate System Model version 4, *J. Clim.*, 24, 4973–4991.
- Gettelman, A., H. Morrison, and S. J. Ghan (2008), A new two moment bulk stratiform cloud microphysics scheme in the Community Atmosphere Model, version 3 (CAM3). Part II: Single-column and global results, *J. Clim.*, 21, 3660–3679.
- Gettelman, A., X. Liu, S. J. Ghan, H. Morrison, S. Park, A. J. Conley, S. A. Klein, J. Boyle, D. L. Mitchell, and J. L. F. Li (2010), Global simulations of ice nucleation and ice supersaturation with an improved cloud scheme in the Community Atmosphere Model, *J. Geophys. Res.*, 115, D18216, doi:10.1029/2009JD013797.
- Gettelman, A., J. E. Kay, and K. M. Shell (2011), The evolution of climate sensitivity and climate feedbacks in the Community Atmosphere Model, *J. Clim.*, 25(5), 1453–1469, doi:10.1175/jcli-d-11-00197.1.
- Govindasamy, B., and K. Caldeira (2000), Geoengineering Earth's radiation balance to mitigate CO<sub>2</sub>-induced climate change, *Geophys. Res. Lett.*, 27(14), 2141–2144, doi:10.1029/1999GL006086.
- Govindasamy, B., S. Thompson, P. B. Duffy, K. Caldeira, and C. Delire (2002), Impact of geoengineering schemes on the terrestrial biosphere, *Geophys. Res. Lett.*, 29(22), 2061, doi:10.1029/2002GL015911.
- Haywood, J. M., A. Jones, N. Bellouin, and D. Stephenson (2013), Asymmetric forcing from stratospheric aerosols impacts Sahelian rainfall, *Nat. Clim. Change*, 3(7), 660–665, doi:10.1038/nclimate1857.
- Hunke, E., and W. H. Lipscomb (2010), CICE: The Los Alamos Sea Ice Model, documentation and software user's manual, version 4.1, *Tech. Rep. LA-CC-06-012*, T-3 Fluid Dynamics Group, Los Alamos National Laboratory.
- Hurrell, J. W., et al. (2013), The Community Earth System Model: A framework for collaborative research, *Bull. Am. Meteorol. Soc.*, 94(9), 1339–1360, doi:10.1175/bams-d-12-00121.1.
- Iacono, M. J., J. S. Delamere, E. J. Mlawer, M. W. Shephard, S. A. Clough, and W. D. Collins (2008), Radiative forcing by long-lived greenhouse gases: Calculations with the AER radiative transfer models, *J. Geophys. Res.*, 113, D13103, doi:10.1029/2008JD009944.
- Ikawa, M., and K. Saito (1990), Description of the non hydrostatic model developed at the Forecast Research department at MRI, *Tech. Rep. MRI*, 28, Japan Meteorol. Agency, Meteor. Res. Inst., Nagamine, Tsukuba-City, Ibaraki, Japan.
- Intergovernmental Panel on Climate Change (1999), Aviation and the global atmosphere, in *Intergovernmental Panel on Climate Change*, edited by J. E. Penner et al., 373 pp., Cambridge Univ. Press, Cambridge, U. K.
- Jakob, C. (2002), Ice clouds in numerical weather prediction models—Progress, problems and prospects, in *Cirrus*, edited by D. K. Lynch et al., pp. 327–345, Oxford Univ. Press, New York.
- Jensen, E. J., et al. (2009), On the importance of small ice crystals in tropical anvil cirrus, *Atmos. Chem. Phys.*, 9(15), 5519–5537, doi:10.5194/acp-9-5519-2009.
- Jiang, J. H., et al. (2012), Evaluation of cloud and water vapor simulations in CMIP5 climate models using NASA “A-Train” satellite observations, *J. Geophys. Res.*, 117, D14105, doi:10.1029/2011JD017237.
- Kärcher, B., and U. Lohmann (2003), The roles of dynamical variability and aerosols in cirrus cloud formation, *Atmos. Chem. Phys.*, 3, 823–838.
- Kravitz, B., et al. (2013), Climate model response from the Geoengineering Model Intercomparison Project (GeoMIP), *J. Geophys. Res. Atmos.*, 118, 8320–8332, doi:10.1002/jgrd.50646.
- Latham, J. (1990), Control of global warming?, *Nature*, 347(6291), 339–340, doi:10.1038/347339b0.
- Lawrence, D. M., et al. (2011), Parameterization improvements and functional and structural advances in version 4 of the Community Land Model, *J. Adv. Model. Earth Syst.*, 3, M03001, doi:10.1029/2011MS000045.
- Lee, E. J., J. G. Jhun, and C. K. Park (2005), Remote connections of the northeast Asian summer rainfall variation revealed by a newly defined monsoon index, *J. Clim.*, 15, 3252–3265.
- Lee, E. J., S. W. Yeh, J. G. Jhun, and B. K. Moon (2006), Seasonal change in anomalous WNPSH associated with the strong East Asian summer monsoon, *Geophys. Res. Lett.*, 33, L21702, doi:10.1029/2006GL027474.
- Lee, S. S., Y. W. Seo, K. J. Ha, and J. G. Jhun (2013), Impact of the western North Pacific subtropical high on the East Asian monsoon precipitation and the Indian Ocean precipitation in the boreal summertime, *Asia-Pac. J. Atmos. Sci.*, 42(2), 171–182.
- Lin, Y. L., R. R. Farley, and H. D. Orville (1983), Bulk parameterization of the snow field in a cloud model, *J. Appl. Meteorol.*, 22, 1065–1092.
- Liu, X., J. E. Penner, S. J. Ghan, and M. Wang (2007), Inclusion of ice microphysics in the NCAR Community Atmospheric Model version 3 (CAM3), *J. Clim.*, 20, 4526–4547.
- Liu, X., et al. (2011), Toward a minimal representation of aerosol direct and indirect effects: Model description and evaluation, *Geosci. Model Dev. Discuss.*, 4(4), 3485–3598, doi:10.5194/gmdd-4-3485-2011.
- Lohmann, U., and E. Roeckner (1995), Influence of cirrus cloud radiative forcing on climate and climate sensitivity in a general circulation model, *J. Geophys. Res.*, 100(D8), 16,305–16,323, doi:10.1029/95JD01383.
- Lu, J., G. A. Vecchi, and T. Reichler (2007), Expansion of the Hadley cell under global warming, *Geophys. Res. Lett.*, 34, L06805, doi:10.1029/2006GL028443.
- Marshall, M. (2013), Get cirrus in the fight against climate change, *New Sci.*, 217(2901), 14.
- Minnis, P., D. F. Young, D. P. Garber, L. Nguyen, W. L. Smith, and R. Palikonda (1998), Transformation of contrails into cirrus during success, *Geophys. Res. Lett.*, 25(8), 1157–1160, doi:10.1029/97GL03314.
- Mitchell, D. L., and W. Finnegan (2009), Modification of cirrus clouds to reduce global warming, *Environ. Res. Lett.*, 4, 045,102.
- Mitchell, D. L., S. Chai, Y. Liu, A. J. Heymsfield, and Y. Y. Dong (1996), Modeling cirrus clouds. Part I: Treatment of bimodal size spectra and case study analysis, *J. Atmos. Sci.*, 53(20), 2952–2966.
- Mitchell, D. L., P. J. Rasch, D. Ivanova, G. M. McFarquhar, and T. Nousiainen (2008), Impacts of small ice crystal assumptions on ice sedimentation rates in cirrus clouds and GCM simulations, *Geophys. Res. Lett.*, 35, L09806, doi:10.1029/2008GL033552.

- Mitchell, D. L., S. Mishra, and R. P. Lawson (2011), Cirrus clouds and climate engineering: New findings on ice nucleation and theoretical basis, in *Planet Earth 2011—Global Warming Challenges and Opportunities for Policy and Practice*, edited by Elias G. Carayannis, 646 pp., InTech, Vienna, Austria.
- Morrison, H., and A. Gettelman (2008), A new two-moment bulk stratiform cloud microphysics scheme in the Community Atmosphere Model, version 3 (CAM3). Part I: Description and numerical tests, *J. Clim.*, *21*, 3642–3659.
- Muri, H., A. Berger, Q. Yin, A. Voldoire, D. S. Méliá, and S. Sundaram (2012), SST and ice sheet impacts on the MIS–13 climate, *Clim. Dyn.*, *39*(7), 1739–1761, doi:10.1007/s00382-011-1216-9.
- Murphy, J. M., D. M. H. Sexton, D. N. Barnett, G. S. Jones, M. J. Webb, M. Collins, and D. A. Stainforth (2004), Quantification of modeling uncertainties in a large ensemble of climate change simulations, *Nature*, *430*, 768–772.
- Neale, R. B., J. Richter, S. Park, P. H. Lauritzen, S. J. Vavrus, P. J. Rasch, and M. Zhang (2013), The mean climate of the Community Atmosphere Model (CAM4) in forced SST and fully coupled experiments, *J. Clim.*, *26*, 5150–5168, doi:10.1175/JCLI-D-12-00326.1.
- Ninomiya, K. (1987), Variation of Baiu precipitation over Japan in 1951–1980 and large-scale characteristics of wet and dry Baiu, *J. Meteorol. Soc. Jpn.*, *65*, 115–127.
- Ninomiya, K., and H. Mizuno (1985), Anomalous cold spell in summer over northeastern Japan caused by northeasterly wind from polar maritime airmass. Part 1. EOF analysis of temperature variation in relation to large-scale situation causing the cold summer, *J. Meteorol. Soc. Jpn.*, *63*, 845–857.
- Ogi, M., K. Yamazaki, and Y. Tachibana (2003), Impact of the wintertime NAO on the summertime atmospheric circulation and its solar cycle modulation, Abstract #OS21B-1126 presented at 2003 Fall Meeting, AGU, Washington, D. C.
- Ogi, M., Y. Tachibana, and K. Yamazaki (2004), The connectivity of the winter North Atlantic Oscillation (NAO) and the summer Okhotsk High, *J. Meteorol. Soc. Jpn.*, *82*(3), 905–913.
- Ojebuoboh, F. K. (1992), Bismuth—Production, properties, and applications, *J. Min. Met. Mat. S.*, *44*(4), 46–49, doi:10.1007/BF03222821.
- Oleson, K. W., et al. (2010), Technical Description of version 4.0 of the Community Land Model (CLM), *Tech. Note NCAR/TN-478+STR*, Natl. Cent. for Atmos. Res., Boulder, Colo.
- Sanderson, B., et al. (2008), Constraints on model response to greenhouse gas forcing and the role of sub-grid scale processes, *J. Sci.*, *21*, 2384–2400.
- Sausen, R., et al. (2005), Aviation radiative forcing in 2000: An update on IPCC (1999), *Meteorol. Z.*, *14*(4), 555–561.
- Schmidt, G. A., R. A. Ruedy, R. L. Miller, and A. A. Lacis (2010), Attribution of the present-day total greenhouse effect, *J. Geophys. Res.*, *115*, D20106, doi:10.1029/2010JD014287.
- Schmidt, H., et al. (2012), Can a reduction of solar irradiance counteract CO<sub>2</sub>-induced climate change?—Results from four Earth system models, *Earth Syst. Dynam. Discuss.*, *3*, 31–72.
- Schröder, F., B. Kärcher, C. Duroure, J. Ström, A. Petzold, J. F. Gayet, B. Strauss, P. Wendling, and S. Borrmann (2000), On the transition of contrails into cirrus clouds, *J. Atmos. Sci.*, *57*(4), 464–480, doi:10.1175/1520-0469(2000)057<0464:OTTOCI>2.0.CO;2.
- Screen, J. A., and I. Simmonds (2010), The central role of diminishing sea ice in recent Arctic temperature amplification, *Nature*, *464*(7293), 1334–1337, doi:10.1038/nature09051.
- Stainforth, D. A., et al. (2005), Uncertainty in predictions of the climate response to rising levels of greenhouse gases, *Nature*, *433*, 403–406.
- Storelvmo, T., J. E. Kristjansson, H. Muri, M. A. Pfeffer, D. Barahona, and A. Nenes (2013), Cirrus cloud seeding has potential to cool climate, *Geophys. Res. Lett.*, *40*, 178–182, doi:10.1002/grl.50122.
- Thompson, D. W. J., and J. M. Wallace (1998), The Arctic Oscillation signature in the wintertime geopotential height and temperature fields, *Geophys. Res. Lett.*, *25*(9), 1297–1300, doi:10.1029/98GL00950.
- Tilmes, S., et al. (2013), The hydrological impact of geoengineering in the Geoengineering Model Intercomparison Project (GeoMIP), *J. Geophys. Res. Atmos.*, *118*, 11,036–11,058, doi:10.1002/jgrd.50868.
- Tomassini, L., E. P. Gerber, M. P. Baldwin, F. Bunzel, and M. Giorgetta (2012), The role of stratosphere-troposphere coupling in the occurrence of extreme winter cold spells over northern Europe, *J. Adv. Model. Earth Syst.*, *4*, M00A03, doi:10.1029/2012MS000177.
- Wang, B., R. Wu, and X. Fu (2000), Pacific-East Asia teleconnection: How does ENSO affect East Asian climate?, *J. Clim.*, *13*, 1517–1536.
- Wang, C. (2005), *The Hadley Circulation: Present, Past, and Future*, pp. 173–202, chap. ENSO, Atlantic climate variability, and the Walker and Hadley circulations, Kluwer Acad., Dordrecht, Netherlands.
- Wang, J. (1992), Effects of blocking anticyclones in Eurasia in the rainy season (Meiyu/Baiu season), *J. Meteorol. Soc. Jpn.*, *70*, 929–951.
- Wigley, T. M. L. (2006), A combined mitigation/geoengineering approach to climate stabilization, *Science*, *314*, 452–454.
- Wise, M. E., K. J. Baustian, T. Koop, M. A. Freedman, E. J. Jensen, and M. A. Tolbert (2012), Depositional ice nucleation onto crystalline hydrated NaCl particles: A new mechanism for ice formation in the troposphere, *Atmos. Chem. Phys.*, *12*, 1121–1134.